

Characterization of cracks in nonlinear ferromagnetic plate by eddy current testing

Aldjia Chaalani¹; Dahmane Hachi²; Bachir Helifa¹; Mohammed Naidjate^{1,3}; Iben Khaldoun Lefkaier¹; Mouloud Feliachi³.

¹ Laboratoire de Physique des Matériaux, Université de Laghouat, BP 37G, Laghouat 03000, Algeria

²Laboratory of Development in Mechanics and Materials (LDMM), University of Djelfa, PB 3117, Djelfa, Algeria.

³IREENA-IUT, University of Nantes - UNAM, CRTT, BP 406, 44602 Saint-Nazaire cedex, France,

Abstract: In this work, we aim to determine the dimensions of an axisymmetric crack contained in a non-linear magnetic material. First, we begin to characterize the magnetic material from a modeling of the direct magnetodynamic problem by 2D finite element of the system (magnetic material + sensor) and solved by the Newton Rapheson method. FEMM(Finite Element Method Magnetics, an open source software, was used to validate the model).This direct model is then inverted by a simplex algorithm to determine the dimensions of the crack.

KEYWORDS: Characterization, crack, finite element method, open source FEMM software, inverse problem.

1. Introduction

In industrial Non-Destructive Testing NDT applications, magnetic methods are commonly used to test heat exchangers, welds, pipelines, and other components to assure continued operation and avoid undesirable scenarios. Eddy Current Testing ECT is one of them. are considered to be cheaper and faster compared with traditional destructive tests (Shih, Wang, Wei, & Chen, 2015), (Rosado, Janeiro, Ramos, & Piedade, 2013)

Eddy current testing ECT (Khan & Nusair Khan, 2016) has already been proven to be

effective in detecting cracks in conductive materials (MIX, 2005) (Raj, Jayakumar, & Thavasimuthu, 2007). To induce eddy currents inside a specimen, a coil driven by alternating current is used in traditional eddy current testing. A magnetic field sensor, such as a giant magnetoresistance (GMR) sensor (Pasadas, Ribeiro, Ramos, & Rocha, 2017), Hall sensor (He, et al., 2010) (Tian, Sophian, Taylor, & Rudlin, 2005), or sensing coil (Ribeiro & Ramos, 2008) is used to measure the magnetic field, which is the vector sum of the magnetic field produced by the current running in the excitation coil and the field produced by eddy currents in the specimen. A crack will cause the magnetic field to be perturbed by changing the route of the eddy currents. The magnetic field sensor can detect this disruption, indicating the presence of fissures (Vuillermoz, 1994).

Simulation techniques can be utilized in this context to increase the comprehension of experimental signals, sensor design optimization, NDT performance evaluation, and/or fracture characterization in these materials (Abascal, Lambert, & Lesselier, 2009) (Huang, Takagi, & Uchimoto, 2003).

The work presented in this paper is a contribution to the characterisation of a non-linear magnetic plate and its behaviour under an applied magnetic field. The aim of this

study is to develop a nonlinear model adapted to the resolution of low frequency problems, to better understand the interaction between the magnetic field and the nonlinear magnetic material and to characterise the axisymmetric cracks present in this type of material.

the magnetic permeability of ferromagnetic materials is nonlinear and can be expressed by a curve called the first magnetization curve. In this paper, we will determine the dimensions of axisymmetric crack in a piece of AISI 416. This study differs from others in that we will express the magnetic permeability of this material using the full first magnetization curve, unlike the rest of the studies that express the magnetic permeability of this material is of a constant value, that is, it is considered the permeability of ferromagnetic materials are linear.

In the course of this work, an open source software FEMM (Finite Element Method Magnetics) (Meeker) (Kada Kloucha, 2011) was used to validate the results obtained by the model developed by the finite element method in a Matlab environment.

2. System modelling

The AV nodal formulation is the most often used for the CND-CF problem because of its generality, robustness, and ease of implementation without any restrictions on the continuity requirements (Rachek & Féliachi, 2007).

$$\text{rot}(v \cdot \text{rot}(\vec{A})) + \sigma \left(\frac{\partial \vec{A}}{\partial t} \right) = \vec{J}_s \quad (1)$$

When the direction e_φ it is the azimuthal component A_φ of the vector \vec{A} in such a configuration the currents are perpendicular to the plane of the study (r, z) . the different vector quantities can be written follows

$$\vec{J}_s : \begin{pmatrix} 0 \\ J_\varphi \\ 0 \end{pmatrix} \begin{matrix} \vec{e}_r \\ \vec{e}_\varphi \\ \vec{e}_z \end{matrix} \quad \vec{E} : \begin{pmatrix} 0 \\ E_\varphi \\ 0 \end{pmatrix} \begin{matrix} \vec{e}_r \\ \vec{e}_\varphi \\ \vec{e}_z \end{matrix} \quad \vec{A} : \begin{pmatrix} 0 \\ A_\varphi \\ 0 \end{pmatrix} \begin{matrix} \vec{e}_r \\ \vec{e}_\varphi \\ \vec{e}_z \end{matrix} \quad \vec{B} : \begin{pmatrix} B_r \\ 0 \\ B_z \end{pmatrix} \begin{matrix} \vec{e}_r \\ \vec{e}_\varphi \\ \vec{e}_z \end{matrix} \quad \vec{H} : \begin{pmatrix} H_r \\ 0 \\ H_z \end{pmatrix} \begin{matrix} \vec{e}_r \\ \vec{e}_\varphi \\ \vec{e}_z \end{matrix}$$

As the A vector is merged with its A_φ component, its divergence is therefore naturally zero (Coulomb gauge) $\text{div} \vec{A} = 0$

$$\text{rot}(v \cdot \text{rot} \vec{A}) = \left[-\frac{\partial}{\partial r} \left(v \frac{\partial (r A_\varphi)}{\partial r} \right) - \frac{\partial}{\partial z} \left(v \frac{\partial A_\varphi}{\partial z} \right) \right] \vec{e}_\varphi \quad (2)$$

We replace the expression $r A_\varphi = r A$ with the expression A^*

Because permeability is dependent on magnetic induction in the nonlinear case, the magnetodynamic formulation becomes more complicated.:

$$\left(\frac{\partial}{\partial z} \left(\frac{v(B)}{r} \cdot \frac{\partial A^*}{\partial z} \right) + \frac{\partial}{\partial r} \left(\frac{v(B)}{r} \cdot \frac{\partial A^*}{\partial r} \right) \right) - \frac{\sigma}{r} \frac{\partial A^*}{\partial t} = -J_s \quad (3)$$

A^* is the magnetic vector potential

It's a partial differential equation that describes how an axisymmetric device behaves.

For complicated electromagnetic systems, this formulation can not be solved analytically. As a result, we must utilize a numerical solution approach, and we have chosen the finite element method

2.1. Nodal approximation by the finite element method

The finite element method (Zienkiewicz, 1971) is one of the most suitable methods for solving numeric of partial differential equations. It applies to most problems practices (linear or non-linear, stationary or time-dependent) defined in a any geometric domain in one, two or three dimensions (Feliachi, 1981) (Ren, 1999) (Renhart & Magele, 1990) (Sun, et al., 1992)

The basic concepts of FEM are presented in this part, with an emphasis on the sequence of tasks that assure the computation process' coherence. The method's well-known idea is to discretize the research domain into several parts and then solve the equations associated with the chosen formulation locally in each of them.

A linear combination, weighted by interpolation polynomials, is then used to define the elementary unknowns. The degree of these polynomials and the fineness of the mesh affect the calculation's accuracy. Their coefficients are solely determined by the geometry and discretization of the geometry. Finally, following assembly, a matrix system of equations corresponding to the structure to be analyzed is created, which is straightforward to numerically process. As a result, the finite element method has four main steps.

1. The domain is discretized into a finite number of elements (the mesh) (Touzot & Dhatt, 2005).
2. Discretization of a typical element's partial differential equation (Matthew & Sadiku, 2001).
3. Putting all of the pieces together in the field.
4. Solving the algebraic system that results.

We acquired the following system of nonlinear equations after applying the preceding procedures, and we used Newton Raphson's approach to solve the resulting system of equations (NAÏDJATE, 2012).

$$\frac{v}{4\Delta} \begin{pmatrix} M_{ii} & M_{ij} & M_{ik} \\ M_{ji} & M_{jj} & M_{jk} \\ M_{ki} & M_{kj} & M_{kk} \end{pmatrix} \begin{pmatrix} A_i^* \\ A_j^* \\ A_k^* \end{pmatrix} + j\omega\sigma \frac{\Delta}{12} \begin{pmatrix} 2 & 1 & 1 \\ 1 & 2 & 1 \\ 1 & 1 & 2 \end{pmatrix} \begin{pmatrix} A_i^* \\ A_j^* \\ A_k^* \end{pmatrix} = \frac{\Delta}{3} \begin{pmatrix} J_e \\ J_e \\ J_e \end{pmatrix} \quad (4)$$

Resolution by Newton-Raphson method

We consider the following multidimensional nonlinear system of equations, from the nonlinear equation that depends on (x_1, x_2, \dots, x_n) (Bargallo, 2006):

$$F(x) = \begin{bmatrix} f_1(x_1, x_2, \dots, x_n) \\ f_2(x_1, x_2, \dots, x_n) \\ f_3(x_1, x_2, \dots, x_n) \end{bmatrix} = 0 \quad (5)$$

The Taylor expansion of the function $F(x)$ leads to the following relationship:

$$x^1 = x^0 - \frac{f(x^0)}{\left. \frac{df}{dx} \right|_{x=x^0}} \quad (6)$$

$$x^2 = x^1 - \frac{f(x^1)}{\left. \frac{df}{dx} \right|_{x=x^1}} \quad (7)$$

$$J(x)\{x^{k+1} - x^k\} = -F(x^k)$$

Where $J(x)$ is a Jacobi matrix given by (Bargallo, 2006) :

$$x^{k+1} = x^k - J^{-1}(x).F(x) \quad (8)$$

$$x^{k+1} - x^k = -J^{-1}(x).F(x)$$

$$\Delta x^{k+1} = -J^{-1}(x).F(x)$$

$$J(x) = \begin{bmatrix} \frac{\partial f_1}{\partial x_1} & \frac{\partial f_1}{\partial x_2} & \dots & \frac{\partial f_1}{\partial x_n} \\ \frac{\partial f_2}{\partial x_1} & \frac{\partial f_2}{\partial x_2} & \dots & \frac{\partial f_2}{\partial x_n} \\ \dots & \dots & \dots & \dots \\ \frac{\partial f_n}{\partial x_1} & \frac{\partial f_n}{\partial x_2} & \dots & \frac{\partial f_n}{\partial x_n} \end{bmatrix} \quad (9)$$

We will apply this method to the non-linear part of equation (4) (Bargallo, 2006):

This equation can be written as follows:

$$F = \begin{pmatrix} f_1 \\ f_2 \\ f_3 \end{pmatrix} = \frac{v}{4\Delta} \begin{pmatrix} M_{ii} & M_{ij} & M_{ik} \\ M_{ji} & M_{jj} & M_{jk} \\ M_{ki} & M_{kj} & M_{kk} \end{pmatrix} \begin{pmatrix} A_i^* \\ A_j^* \\ A_k^* \end{pmatrix} + j\omega\sigma \frac{\Delta}{12} \begin{pmatrix} 2 & 1 & 1 \\ 1 & 2 & 1 \\ 1 & 1 & 2 \end{pmatrix} \begin{pmatrix} A_i^* \\ A_j^* \\ A_k^* \end{pmatrix} - \frac{\Delta}{3} \begin{pmatrix} J_e \\ J_e \\ J_e \end{pmatrix} = 0 \quad (10)$$

The first row of the Jacobi matrix can be written as follows (Chaalani, 2017):

$$\frac{\partial f_1}{\partial A_i^*} \Delta A_i^* + \frac{\partial f_1}{\partial A_j^*} \Delta A_j^* + \frac{\partial f_1}{\partial A_k^*} \Delta A_k^* = -f_1$$

$$\frac{v}{4\Delta} [M_{ii} \Delta A_i^* + M_{ij} \Delta A_j^* + M_{ik} \Delta A_k^*] + \frac{1}{4\Delta} (M_{ii} A_i^* + M_{ij} A_j^* + M_{ik} A_k^*) \frac{\partial v}{\partial B^2} \left[\frac{\partial B^2}{\partial A_i^*} \Delta A_i^* + \frac{\partial B^2}{\partial A_j^*} \Delta A_j^* + \frac{\partial B^2}{\partial A_k^*} \Delta A_k^* \right] + j\omega\sigma \frac{\Delta}{12} (2\Delta A_i^* + \Delta A_j^* + \Delta A_k^*) = -\frac{v}{4\Delta} [M_{ii} A_i^* + M_{ij} A_j^* + M_{ik} A_k^*] - j\omega\sigma \frac{\Delta}{12} (2A_i^* + A_j^* + A_k^*) + \frac{\Delta}{3} J_e \quad (11)$$

The same is done for the second and third equations to obtain the following general form:

Then the magnetodynamic model can be written by the N-R method as follows (Chaalani, 2017)

$$\frac{v}{4\Delta} \begin{pmatrix} M_x & M_y & M_z \\ M_y & M_y & M_z \\ M_x & M_y & M_z \end{pmatrix} \begin{pmatrix} \Delta A'_i \\ \Delta A'_j \\ \Delta A'_k \end{pmatrix} + \frac{1}{4\Delta} \frac{\partial v}{\partial B^2} \begin{pmatrix} \sum_{i=1}^n M_{xx} A'_i & \sum_{i=1}^n M_{yy} A'_i & \sum_{i=1}^n M_{zz} A'_i \\ \sum_{i=1}^n M_{yx} A'_i & \sum_{i=1}^n M_{yy} A'_i & \sum_{i=1}^n M_{yz} A'_i \\ \sum_{i=1}^n M_{xz} A'_i & \sum_{i=1}^n M_{yz} A'_i & \sum_{i=1}^n M_{zz} A'_i \end{pmatrix} \begin{pmatrix} \frac{\partial B^2}{\partial A'_i} & 0 & 0 \\ 0 & \frac{\partial B^2}{\partial A'_j} & 0 \\ 0 & 0 & \frac{\partial B^2}{\partial A'_k} \end{pmatrix} \begin{pmatrix} \Delta A'_i \\ \Delta A'_j \\ \Delta A'_k \end{pmatrix} \quad (12)$$

$$+ j\sigma\omega \frac{\Delta}{12} \begin{pmatrix} 2 & 1 & 1 \\ 2 & 1 & 1 \\ 2 & 1 & 1 \end{pmatrix} \begin{pmatrix} \Delta A'_i \\ \Delta A'_j \\ \Delta A'_k \end{pmatrix} = -\frac{v}{4\Delta} \begin{pmatrix} M_x & M_y & M_z \\ M_y & M_y & M_z \\ M_x & M_y & M_z \end{pmatrix} \begin{pmatrix} A'_i \\ A'_j \\ A'_k \end{pmatrix} - j\sigma\omega \frac{\Delta}{12} \begin{pmatrix} 2 & 1 & 1 \\ 2 & 1 & 1 \\ 2 & 1 & 1 \end{pmatrix} \begin{pmatrix} A'_i \\ A'_j \\ A'_k \end{pmatrix} + \frac{\Delta}{3} J_s \begin{pmatrix} 1 \\ 1 \\ 1 \end{pmatrix}$$

Such as v is the magnetic reluctivity of a nonlinear magnetic material depends on the magnetic field.

$$\mathcal{G}(B) = \frac{1}{\mu(B)} \quad (13)$$

Now we can develop a model to solve the equation (12) using Matlab® program in order to calculate \vec{A} . It should be noted here that B in equation (12) is calculated as follows:

$$\vec{B} = \text{rot} \vec{A}$$

$$B^2 = \left(\frac{\partial A^*}{\partial x} \right)^2 + \left(\frac{\partial A^*}{\partial y} \right)^2 \quad (14)$$

$$A^* = \frac{1}{2\Delta} (a_i + b_i x + c_i y) A'_i + \frac{1}{2\Delta} (a_j + b_j x + c_j y) A'_j + \frac{1}{2\Delta} (a_k + b_k x + c_k y) A'_k$$

$$\frac{\partial A^*}{\partial x} = \frac{A'_i b_i + A'_j b_j + A'_k b_k}{2\Delta}$$

$$\frac{\partial A^*}{\partial y} = \frac{A'_i c_i + A'_j c_j + A'_k c_k}{2\Delta}$$

$$B^2 = \left(\frac{A'_i b_i + A'_j b_j + A'_k b_k}{2\Delta} \right)^2 + \left(\frac{A'_i c_i + A'_j c_j + A'_k c_k}{2\Delta} \right)^2 = \frac{(A'_i b_i + A'_j b_j + A'_k b_k)^2 + (A'_i c_i + A'_j c_j + A'_k c_k)^2}{4\Delta^2}$$

$$\frac{\partial B^2}{\partial A'_i} = \frac{2b_i (A'_i b_i + A'_j b_j + A'_k b_k) + 2c_i (A'_i c_i + A'_j c_j + A'_k c_k)}{4\Delta^2}$$

3. Characterisation of an axisymmetric crack in a non-linear magnetic material

3.1. direct model

The magnetic permeability of a nonlinear magnetic material depends on the magnetic field and is given by equation (Brauer, 2013) (BRAUER, 1975):

$$\mu = B / H = \left[1 / \left(k_1 e^{k_2 B^2} + k_3 \right) \right] + \mu_0 \quad (15)$$

- μ is the magnetic permeability of the non-linear magnetic material.
- \vec{H} is a magnetic field applied to the plate "excitation"

- \vec{B} The magnetic induction is the "plate response".

k_1, k_2 and k_3 are parameters related to the type of material. For each ferromagnetic material, the first magnetisation curve depends on the three parameters k_1, k_2 and k_3

Our study about AISI 416 steel which has the following coefficients (Brauer, 2013) :

$$k_1 = 11,92$$

$$k_2 = 2,749$$

$$k_3 = 1036$$

Figure 1 shows the B=f(H) curve, which is the first magnetisation curve for AISI 416 steel.

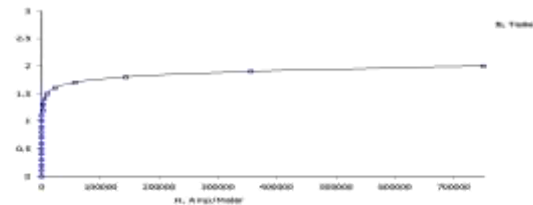


Figure 1 B-H curve for AISI 416 stainless steel

3.1.2. Geometric characteristics

Table 1 shows the system parameters.

Table 1. System parameters

Coil	
Outer radius	10.7mm
Internal radius	6.88mm
Number of turns	410 turns
Height	5mm
Lifte_off	0.19mm
Specimen	
Electrical conductivity	0.175 M [Ωm] ⁻¹
Thickness	1cm
Crack	
Rayon	3mm
Depth	2mm
Other	
Frequency	100 Hz

3.1.3. Discretization of the geometry

In figure 2 the mesh obtained by the elaborated model is presented. In figure 3 the mesh obtained by FEMM is presented.

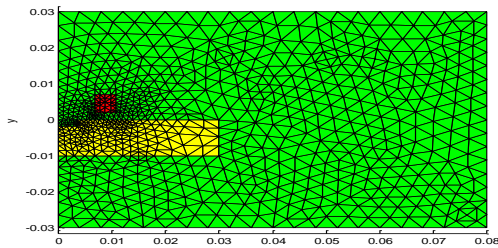


Figure 2 Meshes obtained by the elaborated model

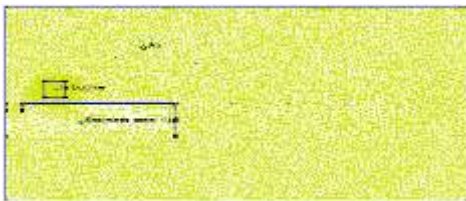


Figure 3 FEMM meshes

It's worth noting that the geometric discretization provided by Matlab differs from that provided by FEMM, We note that FEMM offers much more control and manageability over the type, shape and accuracy of the mesh. Matrices are used to code and store the data generated by the meshing process.

3.1. 4. Magnetic vector potential

Figures 4 and 5 show respectively the iso values of the magnetic vector potential \vec{A} calculated by the developed code and FEMM in an AISI 416 piece. Figure 6 shows the magnetic vector potential distribution.

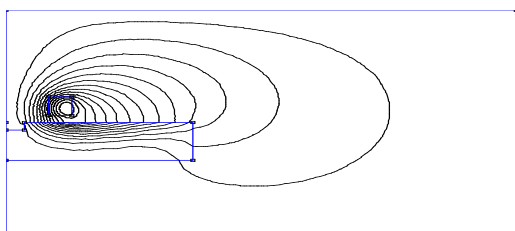


Figure 4 Magnetic vector potential contours by FEM

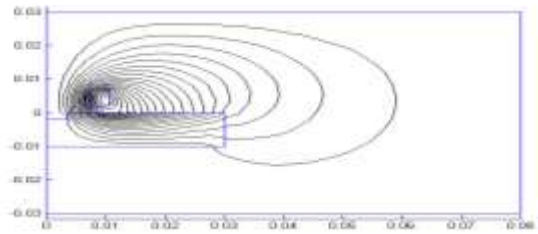


Figure 5 Isovalues of the magnetic vector potential.

3.1.5. Magnetic vector potential

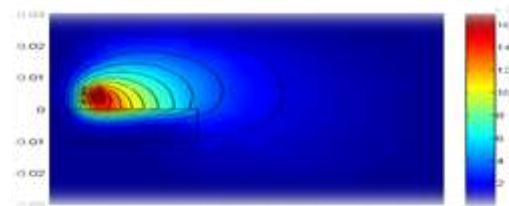


Figure 6 Magnetic vector potential

3.1.6. Magnetic induction B

In figure 7 the magnetic induction B is presented by our model.

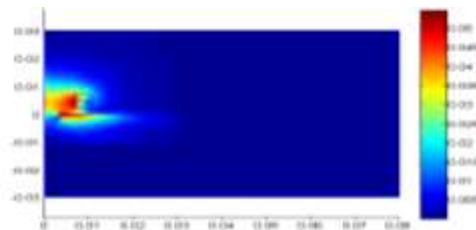


Figure 7 Magnetic induction B

Figure 8 shows the magnetic induction by FEMM.



Figure 8 induction B -magnetic by FEMM

We note that there is good agreement between the two results.

3.1.7. Induced currents

Figure 9 shows the currents induced in the plate by our model with MA / m^2

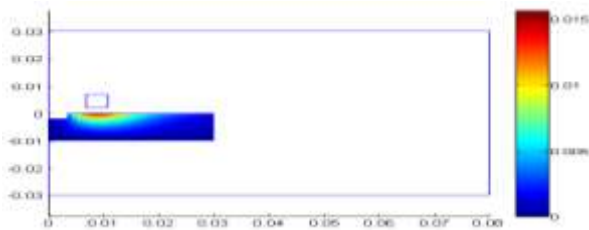


Figure 9 Induced currents

The figure 10 shows the currents induced by FEMM, with MA / m^2



Figure 10 FEMM induced currents in the plate

3.1.8. Impedance calculation

Because our simulation is based on the calculation of the coil's impedance variation (Helifa, 2012), the impedance calculation was used. To begin, we'll need a model that allows us to compute the electromagnetic field both with and without the crack.

$$I^2 \Delta Z = j\omega \int_{\Omega_s} (\vec{A} - \vec{A}_0) \cdot \vec{J}_s d\Omega_s \quad (16)$$

Where \vec{A} and \vec{A}_0 are the magnetic vector potentials with and without the crack respectively (Fukutomi, Takagi, Tani, Hashimoto, Shimone, & Harada, 1997)

I and ω are respectively the intensity and the frequency of the current in the coil.

We calculate the impedance of the system by the developed model and validated it by FEMM.

In table 2 a comparison between the impedance obtained by the developed model and that obtained by FEMM is presented.

Table 2 Comparison between the results

	The real part of Z	The imaginary part of Z
Z with the N-R method	0.0016	2.26
Z by FEMM	0.0017	2.30

3.1.9. Validation of the impedance diagram

Figure 11 shows the normalized impedance diagram calculated by the developed code and its validation by FEMM respectively. These results are obtained at a frequency interval of $[100:400:2000] Hz$

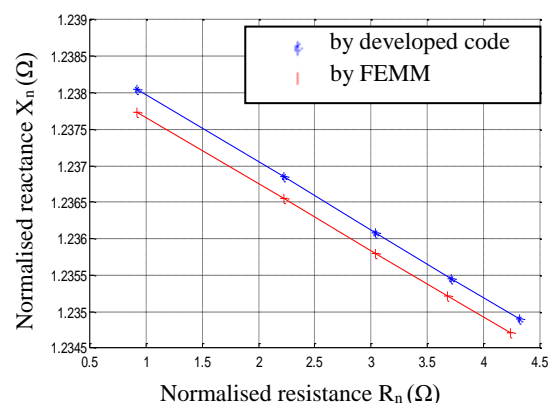


Figure 11 Validation of the impedance diagram

The slight difference between the reactance values can be attributed to the mesh sizes used by the two codes.

3.1. 10. influence of the depth and radius of the crack

To test the sensitivity of the developed model to the variation of the dimensions « radius and depth » of both the 2D axisymmetric crack for an excitation frequency range of $[100 : 200 : 2000] Hz$, we plot the normalised impedance diagram for different values of radius and depth.

The figure12 shows the normalized impedance diagrams.

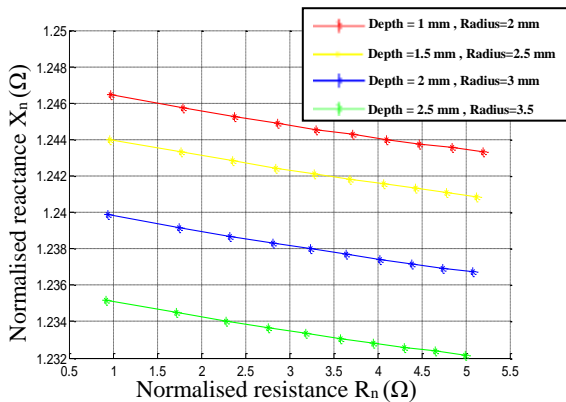


Figure 12 Influence of the geometric of the crack impedance diagram.

It can be seen that the impedance is influenced by the variation of both the depth and the radius of the crack, which shows that the model is sensitive to the variation of the crack dimensions. Thus, the direct model developed can be inverted.

3.2. Inverse problem

The correctness of the direct model is very important in inversion; an erroneous model might result in a poor result.

The direct problem is solved in this paper by discretising the vector potential formulation using a 2D axisymmetric finite element model.

In order to minimize an objective function, the problem is solved by modifying the parameters sought in the simplex iterative process. As a result, we try to keep the difference (or error) between the impedance predicted by the direct model and the impedance measured to a minimum. It should be noted that iterative inversion is highly sensitive to the direct model's accuracy, an inaccurate model may result in an unsatisfying solution.

The choice of the initialization of the estimated characteristics is also important. Indeed, these optimisation algorithms these optimisation algorithms look for minima, and it happens that the result is a local minimum

and not a global one (Helifa, 2012) (Bowler & Huang, 2005) (Doirat, 2007).

Figure 13 illustrates this principle in the case of the non-destructive evaluation of one or several parameters

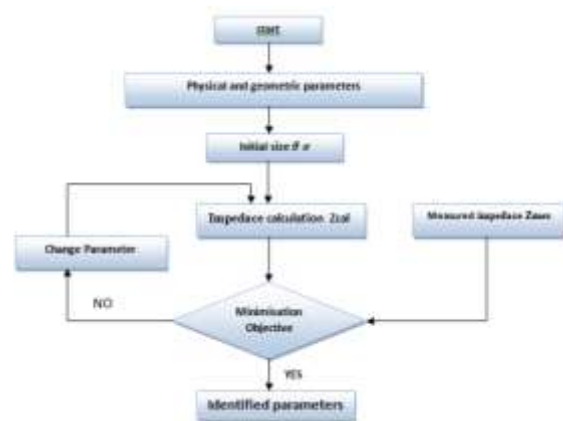


Figure13 Iterative objective function minimization algorithm (Helifa, 2012) (Nelder & Meadf, 1965)

The objective function :

$$F_{obj} = \sqrt{\frac{1}{N_f} \sum_{n=1}^{n=N_f} \left[\left(1 - \frac{R_{cal}(n)}{R_{mes}(n)} \right)^2 + \left(1 - \frac{X_{cal}(n)}{X_{mes}(n)} \right)^2 \right]} \quad (17)$$

Where $R_{cal}(n)$ and $X_{cal}(n)$ are the normalized resistances and reactances calculated with the direct model.

$R_{mes}(n)$ and $X_{mes}(n)$ are the normalised resistances and reactances from the measurements.

N_f is the number of frequencies considered.

This function is minimised using the simplex algorithm (Nelder & Meadf, 1965).

A direct model of the system must then be established to determine $R_{cal}(n)$ and $X_{cal}(n)$.

The blue coloured impedance diagram in figure 12 is used as input vector is considered as experimental values Z_{mes} and the following values as reference values:

- Crack depth = 2 mm
- Crack radius = 3 mm

Figures 14 show the normalised impedance diagram and the variation in crack dimensions for each iteration respectively.

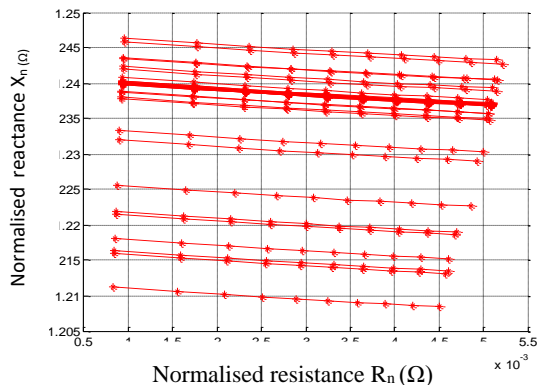


Figure 14 Impedance diagram for each iteration.

In Figure 15 we show the inversion results obtained in this example. It shows the dimension values and the residual value in each iteration until convergence.

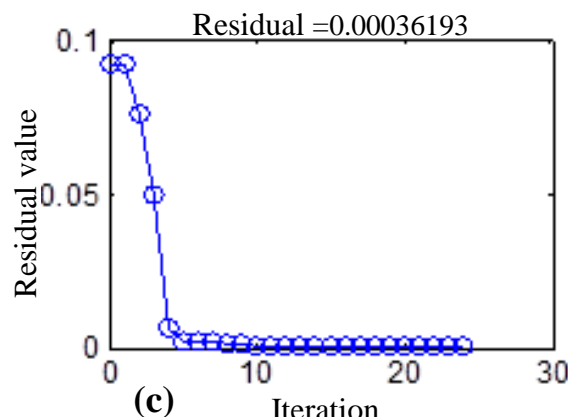
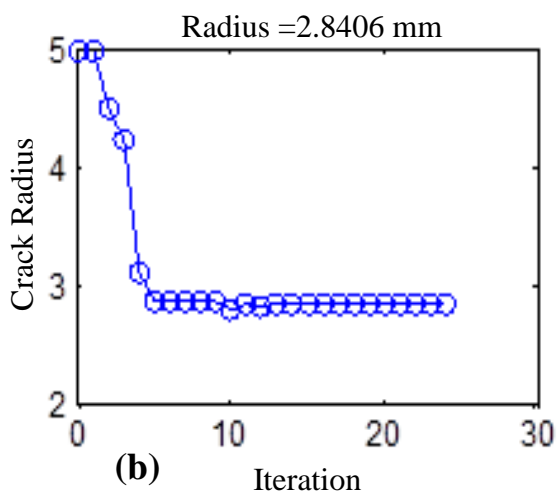
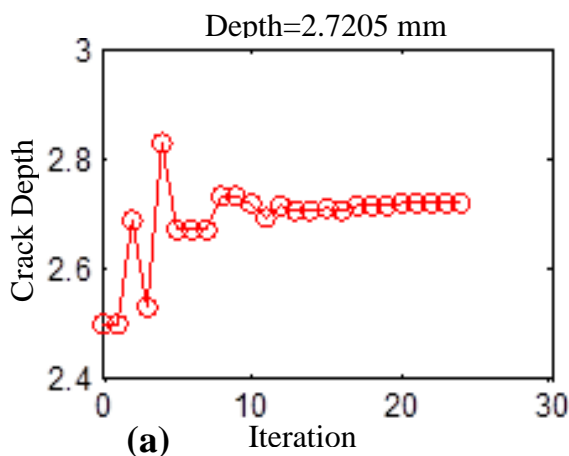


Figure 15 Evolution of the different quantities during iterations, (a) Crack Depth , (b) Crack Radius , (c) Residual value in each iteration

We note that there is, in general, good agreement between the results obtained by inversion and the reference values.

Table 3 Comparison of the obtained and reference values

	Values obtained by inversion	Reference values
crack depth	2.7mm	2mm
crack width	2.8mm	3mm

4. Conclusion

This paper, devoted to the characterisation of an axisymmetric crack in a non-linear magnetic material, was carried out by inverting a developed 2D axisymmetric model with a simplex algorithm to determine the dimensions of a non-through crack. It should be noted here that in the case of axial symmetry, the results of the study in 2D are completely equivalent to the study of 3D, and we resort to 2D to reduce and simplify the calculation period. The normalised impedance diagram allowed us to overcome the uniqueness problem often encountered in solving the inverse problem.

5. Future scope

In the future, we aspire to expand this study by exploiting the two-dimensional program that we developed to characterise some properties of ferromagnetic materials such as the magnetic permeability and Electrical conductivity ...ect .It would also be good to work on determining the dimensions of the no axisymmetric crack that requires a three-dimensional study, that is, we will work on developing 3D finite element program in a Matlab® environment.

6. References

- Abascal, J. F., Lambert, M., & Lesselier, D. (2009). Nonlinearized mapping of volumetric defects affecting a metal tube. Dans *Electromagnetic Nondestructive Evaluation* (Vol. 32, pp. 172-179). IOS Press.
- Bargallo, R. (2006). Finite elements for electrical engineering. Universitat Politecnica De Catalunya.
- Bowler, N., & Huang, Y. (2005). Electrical conductivity measurements of metal plates using broadband eddy current and four point methods. *MEASUREMENT SCIENCE AND TECHNOLOGY*, 16.
- Brauer, J. R. (2013). *Magnetic actuators*.
- BRAUER, J. R. (1975). Simple Equations for the Magnetization. *IEEE Transactions on Magnetics*, 81.
- Chaalani, A. (2017). *Determination of the dimensions of a defect by the nodal finite element method*. these magister, Ecole nationale superieure de laghoute .
- Doirat, V. (2007). Contribution à la modélisation de systèmes de Contrôles Non Destructifs par Courants de Foucault. Application à la caractérisation physique et dimensionnelle de matériaux de l'aéronautique. Doctoral dissertation, Université de Nantes.
- Feliachi, M. (1981). Contribution au calcul du champ électromagnétique par la méthode des. *In These de doctorat* .
- Fukutomi, H., Takagi, T., Tani, J., Hashimoto, M., Shimone, J., & Harada, Y. (1997). Numerical Evaluation of ECT Impedance Signal due to Minute Cracks. *IEEE Transactions On Magnetics*.
- He, Y., Luo, F., Pan, M., Weng, F., Hu, X., Gao, J., et al. (2010). Pulsed eddy current technique for defect detection in aircraft riveted structures. *NDT&E International*, 43(2010)176–181.
- Helifa, B. (2012). Contrubuation a la simulation du CND par courants de foucault en vue de la caractérisation des fisuredébouchan. PhD thesis from the University of Nantes.
- Huang, H., Takagi, T., & Uchimoto, T. (2003). Fast numerical calculation for crack modeling in eddy current testing of ferromagnetic. *Journal of Applied Physics*, 94 (9).
- Kada Kloucha, O. (2011). Etude, réalisation et commande d'un moteur a reluctance. mmoire magister, université d'Oran.
- Khan, S. H., & Nusair Khan, A. (2016). Metallurgical Characterization of Bainitic Steel by Eddy Current. *TECHNICAL ARTICLE_PEER-REVIEWED* .
- Matthew, N., & Sadiku, O. (2001). Numerical Techniques in Electromagnetics 2ed. *CRC Press* (ISBN:0-8493-1395-3).
- Meeker, D. (s.d.). <http://www.femm.info/wiki/HomePage>.
- MIX, P. E. (2005). *Introduction to nondestructive testing a training guide*. (J. W. Sons, Éd.) wiley interscience.
- NAÏDJATE, M. (2012). *Développement d'un Code de Calcul pour l'Etude du Rayonnement*

Electromagnétique des Panneaux Solaires en Champ Proche. Magister thesis , Amar Telidji University Laghouat.

Nelder, J. A., & Mead, R. (1965). A simplex method for function minimization. *The computer journal*, , 7 (4).

Pasadas, D. J., Ribeiro, A. L., Ramos, H. G., & Rocha, T. J. (2017). Inspection of cracks in aluminum multilayer structures using planar ECT probe and inversion problem. *IEEE TRANSACTIONS ON INSTRUMENTATION AND MEASUREMENT*, VOL. 66, NO. 5.

Rachek, M., & Féliachi, M. (2007). 3-D movement simulation techniques using FE methods:. *NDT&E International* .

Raj, B., Jayakumar, T., & Thavasimuthu, M. (2007). *Practical eddy current testing*. Narosa Publishing House.

Ren, Z. (1999). Solving 3-D eddy current problem containing thin cracks using dual. *IEE Proceedings-Science, Measurement and Technology* .

Renhart, W., & Magele, C. A. (1990). The treatment of cracks in NDT problems using FEM. *IEEE Transactions on Magnetism* , 26(2), 873–876.

Ribeiro, A. L., & Ramos, H. G. (2008). Inductive probe for flaw detection in non-magnetic metallic plates using eddy currents. *IEEE Instrumentation and Measurement Technology Conference* . (pp. pp. 1447-1451). IEEE.

Rosado, L., Janeiro, F., Ramos, P., & Piedade, M. (2013). Defect characterization with eddy current testing using nonlinear regression feature extraction. *IEEE Trans Instrum Meas* .

Shih, Y., Wang, Y., Wei, S., & Chen, C. (2015). Improving non-destructive test results using artificial neural networks. *Int J Mach Learn Comput* .

Sun, Y. S., Lin, H. Y., Chen, M. J., De Wang, C., Wu, X. B., Atherton, D., et al. (1992). Finite element modelling and physics of remote field eddy current responses for. *IEEE Transactions on Magnetism* , 28(4), 1941–1947.

Tian, G. Y., Sophian, A., Taylor, D., & Rudlin, J. (2005). Multiple sensors on pulsed eddy-current detection for 3-D subsurface crack assessment. *VOL. 5* (1).

Touzot, G., & Dhatt, G. (2005). *Méthodes Éléments Finis*. Hermès science .

Vuillermoz, P. (1994). Les courants de Foucault. *Principes, mesure et contrôle*, .

Zienkiewicz, O. (1971). *The Finite Element Method in Engineering Science*. New York : McGraw-Hill.